

IMECE2008-66821-DRAFT

SENSOR DIAPHRAGM UNDER INITIAL TENSION: NONLINEAR INTERACTIONS DURING ASYMMETRIC OSCILLATIONS

Xinhua Long

State Key Laboratory of Mechanical System & Vibration, Shanghai Jiao Tong University, Shanghai, 200240, P.R. China, Author for correspondence(PH:(86-21)342-6664, , Email: xhlong@sjtu.edu.cn)

Miao Yu and Balakumar Balachandran

Department of Mechanical Engineering, University of Maryland, College Park, MD 20742-3035.

ABSTRACT

In this article, investigations into the nonlinear asymmetric vibrations of a pressure sensor diaphragm under initial tension are presented. A comprehensive mechanics model based on a plate with in-plane tension is presented and the effect of cubic nonlinearity is studied on the nonlinear asymmetric response when the excitation frequency is close to the natural frequency of an asymmetric mode of the plate. The obtained results show that in the presence of an internal resonance, depending on the initial tension, the response can have not only the form of a standing wave but also the form of a traveling wave. The results of this work should be relevant to diaphragm-type structures used in micro-scale sensors including pressure sensors.

1. INTRODUCTION

Thin film diaphragm structures are frequently used in silicon piezoresistive sensors, capacitive sensors, and fiber-optic sensors [1]-[3]. One can detect the vibrations of these diaphragm structures through the displacements of the diaphragm structures. The sensor sensitivity, bandwidth, and linearity are directly related to the structural behavior of the diaphragm. Due to thermal expansion and mismatch between adjacent wafers, the wafer-bonding operations may introduce in-plane residual stresses in the thin film

diaphragm structures. In a typical silicon pressure sensor, the diaphragm is a stretched thin structure and the initial tension can be as large as 1 GPa [4]. The diaphragm vibrations are usually analyzed by using membrane equations. Static membrane equations have also been used in other sensor designs [1]-[3]. However, as pointed out in the recent work of Yu and Balachandran [5], a membrane model is not always the most appropriate one. Sheplak and Dugundji [6] carried out static analysis of a clamped circular plate under initial tension and studied the transition range from plate behavior to membrane behavior in terms of the tension parameter k . Su, Chen, Roberts, and Spearing. [7] extended this work to analyze large deflections of a pre-tensioned annular plate bonded with a rigid boss under axisymmetric pressure in the presence of in-plane loading. In the work of Yu, Long, and Balachandran, the work presented in [5] is extended to the dynamic case and the tradeoffs between sensitivity, bandwidth, and dynamic range are addressed through a nonlinear analysis.

In most of early research efforts on the dynamic response of a diaphragm structure, harmonic and symmetric excitations are considered. For studying asymmetric responses, Sridhar, Mook, and Nayfeh [9] derived a general solvability condition for nonlinear interactions in the vibrations of a clamped circular plate. Yeo and Lee [10] re-examined a primary resonance state studied by Sridhar *et al.* and corrected the modulation equations derived by Sridhar *et al.* The results

indicate the steady-state response can have not only the form of a standing wave but also the form of a traveling wave. In this paper, the authors follow the work presented in references [9-11] and build on their earlier efforts [5, 8], and carry out a nonlinear analysis of the asymmetric vibrations of a pressure sensor diaphragm under initial tension.

The rest of this article is organized as follows. In the second section, the model of a plate with in-plane tension is provided. In the third section, the equations governing the nonlinear asymmetric vibrations are derived when the system experiences a primary resonance excitation of the one-one mode. Numerical results for three different diaphragm structures are presented in the fourth section. Finally, some remarks are collected together and presented.

2. MODEL DEVELOPMENT AND SYSTEM EQUATIONS

In Figure 1, a clamped, circular diaphragm of radius a and thickness h is illustrated. The Young's modulus of elasticity and Poisson's ratio of the diaphragm material are denoted by E and ν , respectively. The initial tension per unit length applied to the diaphragm is represented by N_0 .

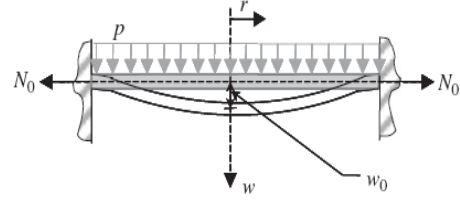
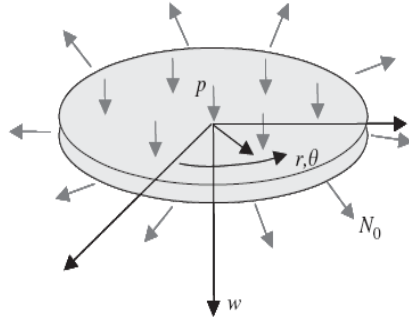


Figure 1: Illustration of a diaphragm clamped along its edge.

A non-dimensional tension parameter k is defined as

$$k = a\sqrt{\frac{N_0}{D}} = \frac{a}{h}\sqrt{\frac{12(1-\nu^2)T}{E}} \quad (1)$$

where the constant $D = Eh^3/(12(1-\nu^2))$ and $T = N_0/h$ is the tension per unit area. In the analysis that follows, it is shown the choice of a plate model or a membrane model actually depends on the tension parameter k , not on just the initial tension per unit length N_0 applied to the diaphragm. Starting from Love's equations (Soedel [12], Nayfeh and Mook [13]), including damping, axial in-plane force per unit length N_r , and the transverse loading per unit area $f(r, \theta; t)$, the nonlinear partial-differential equation governing a plate with initial tension can be obtained as

$$\rho h \frac{\partial^2 w}{\partial t^2} + D \nabla^4 w - N_0 \nabla^2 w = \frac{\partial^2 w}{\partial r^2} \left(\frac{1}{r} \frac{\partial \Phi}{\partial r} + \frac{1}{r^2} \frac{\partial^2 \Phi}{\partial \theta^2} \right) + \frac{\partial^2 \Phi}{\partial r^2} \left(\frac{1}{r} \frac{\partial w}{\partial r} + \frac{1}{r^2} \frac{\partial^2 w}{\partial \theta^2} \right) - 2 \left(\frac{1}{r} \frac{\partial^2 \Phi}{\partial r \partial \theta} - \frac{1}{r^2} \frac{\partial \Phi}{\partial \theta} \right) \left(\frac{1}{r} \frac{\partial^2 w}{\partial r \partial \theta} - \frac{1}{r^2} \frac{\partial w}{\partial \theta} \right) - 2\mu \frac{\partial w}{\partial t} + f(r, \theta; t) \quad (1)$$

$$\nabla^4 \Phi = Eh \left[\left(\frac{1}{r} \frac{\partial^2 w}{\partial r \partial \theta} - \frac{1}{r^2} \frac{\partial w}{\partial \theta} \right)^2 - \frac{\partial^2 w}{\partial r^2} \left(\frac{1}{r} \frac{\partial w}{\partial r} + \frac{1}{r^2} \frac{\partial^2 w}{\partial \theta^2} \right) \right] \quad (2)$$

where r is the radial distance from the center, θ is the angular coordinate, $w(r, \theta; t)$ is the transverse displacement, and μ is the damping coefficient.

For convenience, the authors rewrite these equations in terms of nondimensional variables, denoted by asterisks, which are defined as follows:

$$\begin{aligned}
r &= ar^*, \quad t = a^2 \sqrt{\frac{\rho h}{D}} t^*, \quad w = \frac{h^2}{a} w^*, \\
u &= \frac{h^4}{a^3} u^*, \quad v = \frac{h^4}{a^3} v^*, \quad N_0 = \frac{a^2}{D} N_0^{2*}, \\
\mu &= \frac{24(1-\nu^2)}{a^4} \sqrt{\rho h^5 D} \mu^*, \\
f &= \frac{12(1-\nu^2) Dh^4}{a^7} f^*, \quad \Phi = \frac{Eh^5}{a^2} \Phi^*
\end{aligned} \tag{3}$$

After substituting Eq. (3) into (1) and (2) and dropping the asterisks in the result, one can obtain

$$\begin{aligned}
& \frac{\partial^2 w}{\partial t^2} + \nabla^4 w - N_0 \nabla^2 w \\
&= \varepsilon \left[\frac{\partial^2 w}{\partial r^2} \left(\frac{1}{r} \frac{\partial \Phi}{\partial r} + \frac{1}{r^2} \frac{\partial^2 \Phi}{\partial \theta^2} \right) + \frac{\partial^2 \Phi}{\partial r^2} \left(\frac{1}{r} \frac{\partial w}{\partial r} + \frac{1}{r^2} \frac{\partial^2 w}{\partial \theta^2} \right) \right. \\
& - 2 \left(\frac{1}{r} \frac{\partial^2 \Phi}{\partial r \partial \theta} - \frac{1}{r^2} \frac{\partial \Phi}{\partial \theta} \right) \left(\frac{1}{r} \frac{\partial^2 w}{\partial r \partial \theta} - \frac{1}{r^2} \frac{\partial w}{\partial \theta} \right) \\
& \left. - 2\mu \frac{\partial w}{\partial t} + f(r, \theta; t) \right] \\
& \nabla^4 \Phi = \left[\left(\frac{1}{r} \frac{\partial^2 w}{\partial r \partial \theta} - \frac{1}{r^2} \frac{\partial w}{\partial \theta} \right)^2 - \frac{\partial^2 w}{\partial r^2} \left(\frac{1}{r} \frac{\partial w}{\partial r} + \frac{1}{r^2} \frac{\partial^2 w}{\partial \theta^2} \right) \right]
\end{aligned} \tag{4}$$

where

$$\varepsilon = \frac{12(1-\nu^2)h^2}{a^2} \tag{6}$$

$$\nabla^2 = \frac{\partial^2}{\partial r^2} + \frac{1}{r} \frac{\partial}{\partial r} + \frac{1}{r^2} \frac{\partial^2}{\partial \theta^2} \tag{7}$$

The relationships amongst Φ , w and the in-plane displacements u and v are given by

$$e_1 = \frac{1}{r} \frac{\partial \Phi}{\partial r} + \frac{1}{r^2} \frac{\partial^2 \Phi}{\partial \theta^2} - \nu \frac{\partial^2 \Phi}{\partial r^2} \tag{8}$$

$$e_2 = \frac{\partial^2 \Phi}{\partial r^2} - \nu \left(\frac{1}{r} \frac{\partial \Phi}{\partial r} + \frac{1}{r^2} \frac{\partial^2 \Phi}{\partial \theta^2} \right) \tag{9}$$

$$\frac{1}{2} \gamma_6 = (1+\nu) \frac{1}{r} \left(\frac{1}{r^2} \frac{\partial \Phi}{\partial \theta} - \frac{\partial \Phi}{\partial r \partial \theta} \right) \tag{10}$$

$$e_1 = \frac{\partial u}{\partial r} + \frac{1}{2} \left(\frac{\partial w}{\partial r} \right)^2 \tag{11}$$

$$e_2 = \frac{u}{r} + \frac{1}{r} \frac{\partial v}{\partial \theta} + \frac{1}{2r^2} \left(\frac{\partial w}{\partial \theta} \right)^2 \tag{12}$$

$$\gamma_6 = \frac{1}{r} \frac{\partial u}{\partial \theta} + \frac{\partial v}{\partial r} - \frac{v}{r} + \frac{1}{r} \frac{\partial w}{\partial r} \frac{\partial w}{\partial \theta} \tag{13}$$

The clamped immovable boundary is described by

$$w = 0, \quad \frac{\partial w}{\partial r} = 0, \quad u = 0, \quad \text{and } v = 0 \quad \text{at } r = 1 \tag{14}$$

Making use of equations (8-14), one can obtain the following two conditions on Φ :

$$\frac{\partial^2 \Phi}{\partial r^2} - \nu \left(\frac{1}{r} \frac{\partial \Phi}{\partial r} + \frac{1}{r^2} \frac{\partial^2 \Phi}{\partial \theta^2} \right) = 0 \quad \text{at } r = 1 \tag{15}$$

$$\frac{\partial^3 \Phi}{\partial r^3} + \frac{1}{r} \frac{\partial^2 \Phi}{\partial r^2} - \frac{1}{r^2} \frac{\partial \Phi}{\partial r} + \frac{2+\nu}{r^2} \frac{\partial^3 \Phi}{\partial r \partial \theta^2} - \frac{3+\nu}{r^3} \frac{\partial^2 \Phi}{\partial \theta^2} = 0 \quad \text{at } r = 1 \tag{16}$$

3. NONLINEAR INTERACTIONS: COUPLED OSCILLATOR EQUATIONS

Consider a primary resonance excitation of the n -1th mode having the form

$$F(r, \theta; t) = \hat{f}(r) \cos n\theta e^{i\Omega t} + cc \tag{17}$$

and let the displacement response be approximated as

$$w(r, \theta; t) \approx (\eta(t) \cos n\theta + \zeta(t) \sin n\theta) \phi(r) \tag{18}$$

where

$$\phi(r) = k_{11} \left[\frac{J_1(\beta_{11} r) - \frac{J_1(\beta_{11})}{I_1(\alpha_{11})} I_1(\alpha_{11} r)}{I_1(\alpha_{11})} \right]$$

The coefficient α_{11} and β_{11} are determined by characteristic equations

$$I_1(\alpha_{11}) J_1'(\beta_{11}) - J_1(\beta_{11}) I_1'(\alpha_{11}) = 0 \tag{19}$$

and k_{11} is determined by $1 = \int_0^1 r \phi(r) \phi(r) dr$.

On substituting Eq. (18) into Eq. (5), the result is

$$\nabla^4 \Phi = \frac{1}{2} (\eta^2 + \zeta^2) \chi_1(r) + \left[\frac{1}{2} (\zeta^2 - \eta^2) \cos 2n\theta - \eta \zeta \sin 2n\theta \right] \chi_2(r) \tag{20}$$

where

$$\chi_1 = \frac{n^2}{r^4} (r\phi' - \phi)^2 - \frac{\phi''}{r^4} (r\phi' - n^2 \phi) \tag{21a}$$

$$\chi_2 = \frac{n^2}{r^4} (r\phi' - \phi)^2 + \frac{\phi''}{r^4} (r\phi' - n^2\phi) \quad (21b)$$

The solution of equation (20) that satisfies the boundary conditions can be

$$\Phi = \frac{1}{2} \psi_1(r) (\eta^2 + \zeta^2) + \left[\frac{1}{2} (\zeta^2 - \eta^2) \cos 2n\theta - \eta\zeta \sin 2n\theta \right] \psi_2(r) \quad (22)$$

where ψ_1 and ψ_2 can be expanded in term of the eigenfunctions of

$$\left(\frac{d^2}{dr^2} + \frac{1}{r} \frac{d}{dr} - \frac{4n^2}{r^2} \right)^2 \Psi = \lambda^4 \Psi \quad (23a)$$

$$\Psi'' - \nu \Psi' + 4\nu n^2 \Psi = 0 \quad \text{at } r=1 \quad (23b)$$

$$\Psi''' + \Psi'' - (1 + 8n^2 + 4\nu n^2) \Psi' + 4n^2 (3 + \nu) \Psi = 0$$

$$\text{at } r=1 \quad (23c)$$

$$\Psi(0) < \infty \quad (23d)$$

The solution of equation (23a), which is bounded at the origin, can be expressed as

$$\Psi = c_1 J_{2n}(\lambda r) + c_2 I_{2n}(\lambda r) \quad (24)$$

Imposing the boundary conditions (23b-c) leads to

$$c_1 [\lambda^2 J_{2n}'' - \nu J_{2n}' + 4\nu n^2 J_{2n}] + c_2 [\lambda^2 I_{2n}'' - \nu I_{2n}' + 4\nu n^2 I_{2n}] = 0 \quad (25a)$$

$$c_1 [\lambda^3 J_{2n}''' + \lambda^2 J_{2n}'' - (1 + 8n^2 + 4\nu n^2) \lambda J_{2n}' + 4n^2 (3 + \nu) J_{2n}] + \quad (25b)$$

$$c_2 [\lambda^3 I_{2n}''' + \lambda^2 I_{2n}'' - (1 + 8n^2 + 4\nu n^2) \lambda I_{2n}' + 4n^2 (3 + \nu) I_{2n}] = 0$$

For ψ_1 , $n=0$, and in this case, $n=1$ for ψ_2 . One can determine λ and c_2/c_1 by using equations (27a, b). Then, one has

$$\psi_1 = \sum_{k=1}^{\infty} c_{1k} [J_{20}(\lambda_k r) + c_{2k}/c_{1k} I_{20}(\lambda_k r)] \quad (26a)$$

$$\psi_2 = \sum_{k=1}^{\infty} c_{1k} [J_{2n}(\lambda_k r) + c_{2k}/c_{1k} I_{2n}(\lambda_k r)] \quad (26b)$$

In order to get the coefficients c_{1k} , ψ_1 is multiplied by $c_{1k} r [J_{20}(\lambda_k r) + c_{2k}/c_{1k} I_{20}(\lambda_k r)]$ so that

$$\int_0^1 \left\{ r [J_{20}(\lambda_k r) + c_{2k}/c_{1k} I_{20}(\lambda_k r)] \cdot \sum_{k=1}^{\infty} c_{1k} [J_{20}(\lambda_k r) + c_{2k}/c_{1k} I_{20}(\lambda_k r)] = r [J_{20}(\lambda_k r) + c_{2k}/c_{1k} I_{20}(\lambda_k r)] \chi_1(r) \right\} dr \quad (27)$$

After substituting Eqs. (18) and (22) into Eq. (4), multiplying the outcome with $r\phi(r)\cos\theta$ and $r\phi(r)\sin\theta$, respectively, and integrating the results from $\theta=0$ to $\theta=2\pi$ and $r=0$ to $r=1$, one can obtain the coupled oscillator equations

$$\ddot{\eta} + \omega^2 \eta = -2\varepsilon\mu\dot{\eta} - \varepsilon\alpha_1 \eta^3 - \varepsilon\alpha_2 \eta^2 \zeta - \varepsilon\alpha_3 \eta \zeta^2 - \varepsilon\alpha_4 \zeta^3 + \varepsilon f \cos \Omega t \quad (28a)$$

$$\ddot{\zeta} + \omega^2 \zeta = -2\varepsilon\mu\dot{\zeta} - \varepsilon\alpha_5 \zeta^3 - \varepsilon\alpha_6 \eta \zeta^2 - \varepsilon\alpha_7 \zeta \eta^2 - \varepsilon\alpha_8 \eta^3 \quad (28b)$$

where

$$\alpha_1 = \alpha_3 = \alpha_5 = \alpha_7 = -\int_0^1 \frac{1}{4} \phi [-\psi_2'' \phi' - \psi_2' \phi'' + 2(\psi_1'' \phi' + \psi_1' \phi'')] \quad (29a)$$

$$- \frac{n^2}{r^2} (4\psi_2' \phi + 4\psi_2 \phi') + \frac{n^2}{r} (-2\psi_1'' \phi + 4\psi_2 \phi'' + 4\psi_2' \phi' + \psi_2'' \phi) + \frac{4n^2 \psi_2 \phi}{r^3} \Big] dr$$

$$\alpha_2 = \alpha_4 = \alpha_6 = \alpha_8 = 0 \quad (29b)$$

$$\mu = \int_0^1 r \mu \phi^2 dr \quad \text{and} \quad f = \int_0^1 r f \phi dr \quad (30)$$

4. NUMERICAL RESULTS

As a representative case, a Mylar diaphragm with the Young's modulus of elasticity $E = 3.45 \times 10^9$

Pa, density $\rho = 1.29 \times 10^3 \text{ kg/m}^3$, and Poisson's ratio $\nu = 0.41$ is considered. For a diaphragm radius of 1.75 mm and thickness values of 40 μm , 30 μm , and 20 μm , the dependence of the 1-1 mode natural frequency on the tension parameter k is shown for each of these cases in Figure 2. The natural frequencies increase as the tension parameter k is increased. It is noted that it is possible to get the same 1-1 mode natural frequency (22.87 kHz) as that for a diaphragm with $h=40 \mu\text{m}$ and $k=0$ by choosing the appropriate tension parameters. As pointed out in Figure 2, the tension parameter values are $k=4.6$ and $k=9.12$, for $h=30 \mu\text{m}$ and $h=20 \mu\text{m}$,

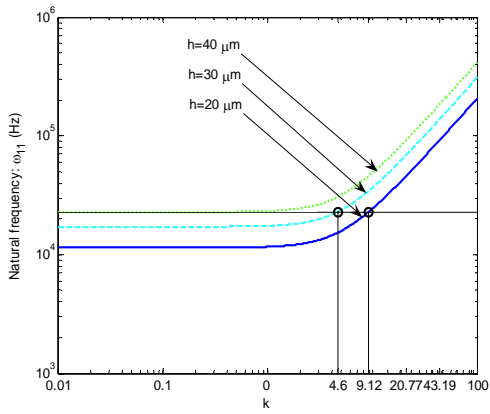


Figure 2. Variation of the natural frequency with respect to the tension parameter for diaphragm structures with different thickness values, for $h=40 \mu\text{m}$, ---- for $h=30 \mu\text{m}$, and — for $h=20 \mu\text{m}$.

In Figure 3, the frequency response curves obtained by using AUTO97 [14] are presented to illustrate the response of structure corresponding to case 1 of Table 1. The corresponding mode has one nodal diameter and no other nodal circle except the one at the boundary. In Figure 3, the branches labeled SS, ST, US, and UT correspond to the stable standing wave, stable traveling wave, unstable standing wave, and unstable traveling wave, respectively. The stable branches and unstable branches are denoted by solid lines and dashed lines, respectively. From Figures 4 and 5, one can find the response of diaphragm transform from a standing wave into a traveling wave with the increase of excitation frequency. The bifurcation point is located at (22975Hz, $3.43 \times 10^{-6} \text{m}$). As the excitation frequency increases, there is one unstable

respectively. The structural and system parameters for the previously mentioned diaphragm structures are provided in Table 1.

Table 1: Structural system parameters and characteristics

Cases	h (μm)	a (mm)	k	f_{11} (Hz)	a_1
1	40	1.75	0	22875	198.9
2	30	1.75	4.6	22875	194.3
3	20	1.75	9.12	22875	177.2

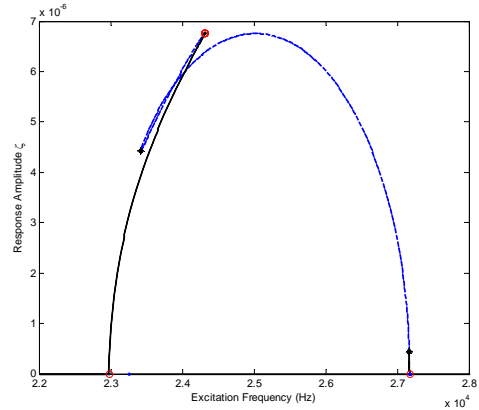
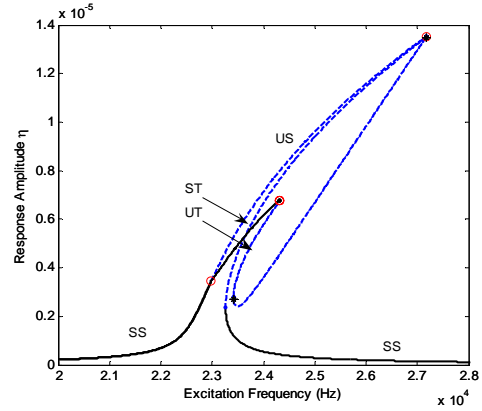


Figure 3. Variations of the diaphragm response amplitudes with respect to the excitation frequency for Case 1 with $k=0$ and pressure $p=100\text{pa}$, ---- unstable branch, — stable branch.

standing wave branch and one stable traveling wave branch in the frequency range (22975Hz, 23264Hz). Following that, the response of diaphragm becomes complicated and there are multiple unstable branches and multiple stable branches in the frequency range (23265Hz, 24312Hz). When the

excitation frequency reaches 24313Hz, there is one stable standing wave branch and multiple unstable branches.

In order to show the deflection of the diaphragm, the responses observed at excitation frequencies of 22500Hz and 23000Hz are considered. The corresponding results obtained by time domain simulations are presented in Figure 4 and 5 to

illustrate the stable responses of the diaphragm over one period of excitation. A standing wave is shown in Figure 4, where one can observe a nodal line in each subplot. In Figure 5, a clockwise rotating traveling wave is shown. The responses shown in Figures 4 and 5 correspond to a primary resonance excitation.

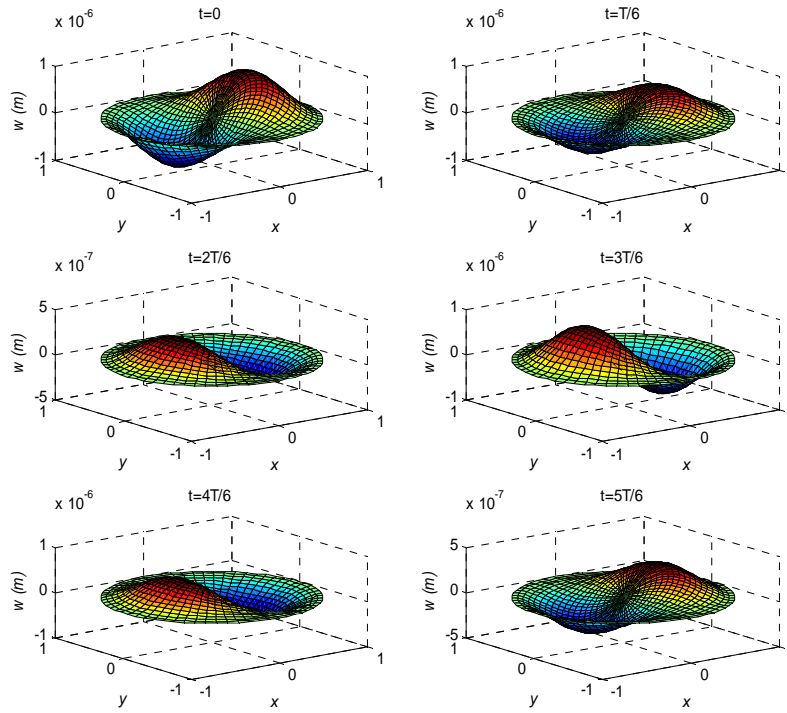


Figure 4. Deflections of the diaphragm in Case 1 over one period of excitation when $\Omega/2\pi = 22500\text{Hz}$ and $p=100\text{Pa}$.

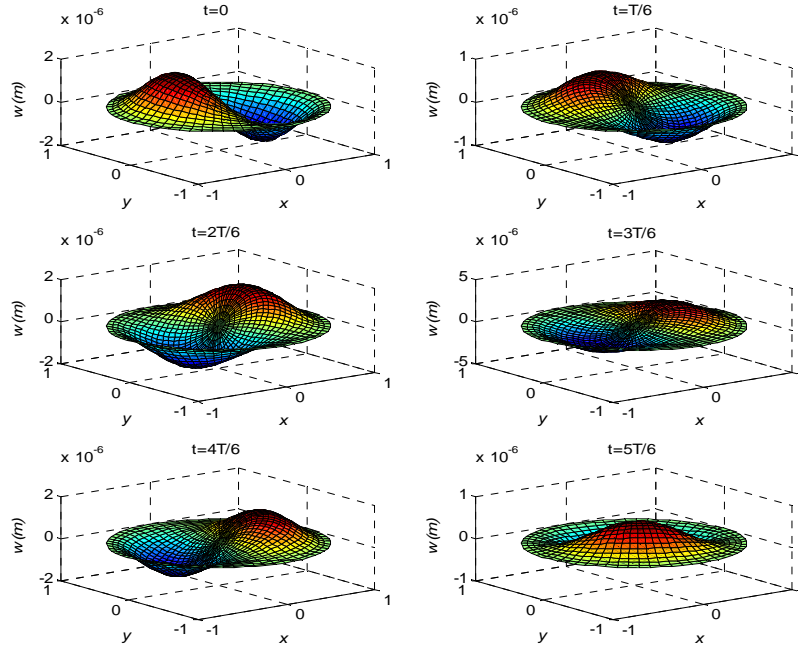


Figure 5. Deflections of the diaphragm in Case 1 over one period of excitation when $\Omega/2\pi = 23000\text{Hz}$ and $p=100\text{Pa}$.

To look into the initial-tension effects on the response of diaphragm, the frequency-response curves obtained for Cases 2 and 3 of Table 1 are presented in Figure 6 and 7. Comparing Figure 6 and 7 with Figure 3, one can find that the branches SS, ST, US, and UT are similar to those of Figure 3. The differences are in the locations of the bifurcation points. In Cases 2 and 3, the first bifurcation points are located at $(22998\text{Hz}, 3.82 \times 10^{-6}\text{m})$ and $(23024\text{Hz}, 4.52 \times 10^{-6}\text{m})$, respectively, as the excitation frequency is increased. One unstable standing wave branch and one stable traveling wave branch are located in the frequency ranges $(23000\text{Hz}, 23352\text{Hz})$ and $(20325\text{Hz}, 23482\text{Hz})$ in Cases 2 and 3, respectively.

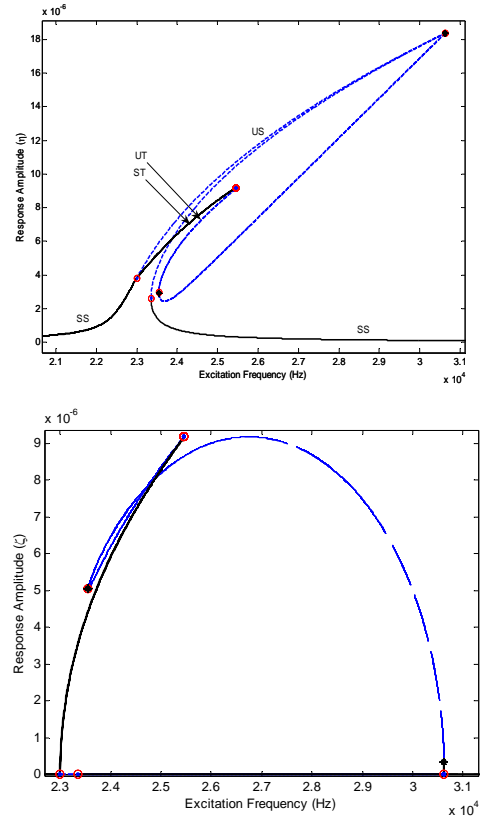


Figure 6. Variations of the diaphragm response

amplitudes with respect to the excitation frequency for Case 2 with $k=4.6$ and pressure $p=100\text{pa}$, --- unstable, — stable branch.

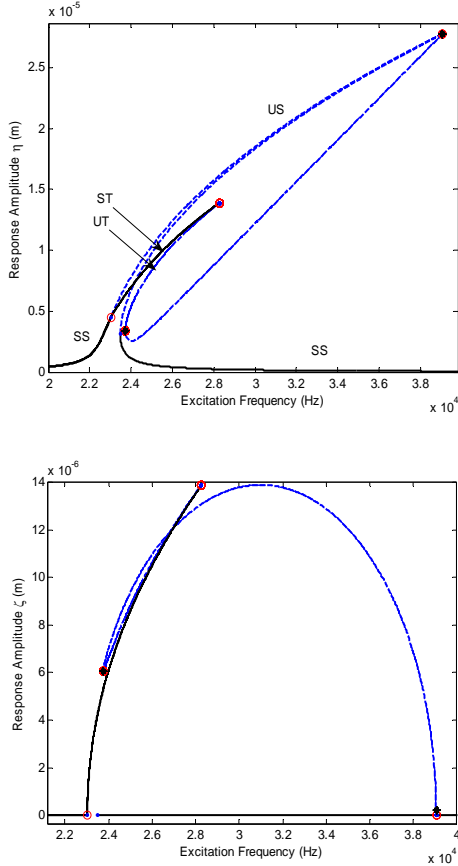


Figure 7. Variations of the diaphragm response amplitudes with respect to the excitation frequency for Case 3 with $k=9.12$ and pressure $p=100\text{pa}$, --- unstable branch, — stable branch,

4. CLOSURE

In this effort, the nonlinear asymmetric vibrations of a pressure sensor diaphragm under initial tension are investigated. A comprehensive mechanics model based on a plate with in-plane tension is presented and the effect of cubic nonlinearity is studied on the nonlinear asymmetric response when the excitation frequency is close to the natural frequency of an asymmetric mode of the plate. The

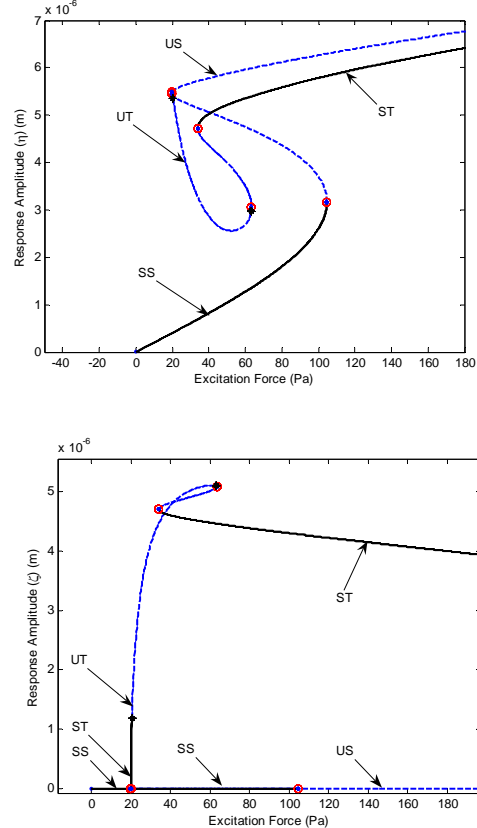


Figure 8. Variations of the diaphragm response amplitudes with respect to the excitation pressure for Case 3 with $k=9.12$ and $\Omega = 23.5 \text{ kHz}$, --- unstable branch, — stable branch.

To investigate nonlinear interactions with respect to the excitation pressure level, the response curves obtained in Case 3 are shown in Figure 8 when the excitation frequency is close to the 1-1 mode natural frequency. From this figure, one can find that stable standing waves occur in the “small” range (0, 20 Pa). With increase of excitation pressure, the responses of diaphragm become complicated and there are multiple stable branches and multiple unstable branches in the range (20 Pa, 100 Pa).

obtained results show that in the presence of an internal resonance, the bifurcation locations depending on the initial tension. The response can have not only the form of a standing wave but also the form of a traveling wave.

REFERENCES

1. Matsuoka, Y., Yamamoto, Y., Tanabe, M., Shimada, S., Yamada, K., Yaskuwa, A., and H. Matsuzaka, (1995), “Low-pressure measurement limits for silicon

- piezoresistive circular diaphragm sensors,” *Journal of Micromechanics and Microengineering*, Vol. 5, pp. 32-35.
2. Pedersen, M., Meijerink, M. G. H., Olthuis, W., and Bergveld, P., (1997), “A capacitive differential pressure sensor with polyimide diaphragm,” *Journal of Micromechanics and Microengineering*, Vol. 7, pp. 250—252.
 3. Zeng, N., Shi, C., Wang, D., Zhang, M., and Y. Liao, (2003), “Diaphragm-type fiber-optic interferometric acoustic sensor,” *Optical Engineering*, Vol. 42(9), pp. 2558—2562.
 4. Cho, S. T. Najafi, K, and Wise, K. D., (1992), “Internal Stress Compensation and Scaling in Ultrasensitive Silicon Pressure Sensor,” *IEEE Transaction on Electron Devices*, Vol. 39, pp. 836-840.
 5. Yu, M. and Balachandran, B. (2005), “Sensor diaphragm under initial tension: Linear analysis,” *Experimental Mechanics*, Vol. 45, pp.123-129.
 6. Sheplak, M. and Dugundji, J. (1998), “Large deflections of clamped circular plates under initial tension and transitions to membrane behavior,” *ASME Journal of Applied Mechanics*, Vol. 65, pp. 107—115.
 7. Su, Y.H., Chen, K.S., Roberts, D.C., and Spearing S. M., (2001), “Large deflection analysis of a pre-stressed annular plate with a rigid boss under axisymmetric loading,” *Journal of Micromechanics and Microengineering*, Vol. 11, pp. 645-653.
 8. Yu, M., Long, X.-H., and Balachandran, B., (2008), “Sensor diaphragm under initial tension: Nonlinear responses and design implications,” *Journal of Sound and Vibration*, Vol. 312, pp. 39-54.
 9. Sridhar, S, Mook, D. T., and Nayfeh, A. H., (1978), “Nonlinear resonances in the forced responses of plates. Part II: asymmetric responses of circular plates,” *Journal of Sound and Vibration*, Vol. 59, pp. 159-170.
 10. Yeo, M. H. and Lee, W. K., (2002), “Corrected solvability conditions for non-linear asymmetric vibrations of a circular plate,” *Journal of Sound and Vibration*, Vol. 257, pp. 653-665.
 11. Nayfeh, A. H. and Pai, P. F., (2004), *Linear and Nonlinear Structural Mechanics*, Wiley, New York.
 12. Nayfeh, A. H. and Mook, D. T., (1979), *Nonlinear Oscillations*, Wiley, New York.
 13. Soedel, W., (1993), *Vibrations of Shells and Plates*, Marcel Dekker, New York.
 14. Doedel, E. J., Champneys, A. R., Fairgrieve, T. F., Kuznetsov, Y. A., Sandstede, B., and Wang, X., (1997), *AUTO97: Continuation and Bifurcation Software for Ordinary Differential Equations (with HOMCONT)*, Technical Report, Concordia University.